

Geometry-dependent Casimir forces on a silicon chip

J. Zou,^{1,2} Z. Marcet,^{1,2} A. W. Rodriguez,^{3,4} M. T. H. Reid,⁵ A. P. McCauley,⁶

I. I. Kravchenko,⁷ T. Lu,² Y. Bao,¹ S. G. Johnson,⁴ and H. B. Chan^{2,*}

¹*Department of Physics, University of Florida, Gainesville, Florida 32611, USA*

²*Department of Physics, the Hong Kong University of Science and Technology,
Clear Water Bay, Kowloon, Hong Kong, China*

³*School of Engineering and Applied Sciences,
Harvard University, Cambridge, Massachusetts 02138, USA*

⁴*Department of Mathematics, Massachusetts Institute of Technology,
Cambridge, Massachusetts 02139, USA*

⁵*Research Laboratory of Electronics,
Massachusetts Institute of Technology,
Cambridge, Massachusetts 02139, USA*

⁶*Department of Physics, Massachusetts Institute of Technology,
Cambridge, Massachusetts 02139, USA*

⁷*Center for Nanophase Materials Sciences,
Oak Ridge National Laboratory, Oak Ridge, Tennessee 37830, USA*

Abstract

We report measurements of the Casimir force gradient between two parallel silicon beams with near-square cross sections at separations down to ~ 260 nm. Both the force-sensing element and the actuator that controls the distance are integrated on the same substrate, with no need for manual alignment. Taking residual electrostatic forces into consideration, the measured Casimir force gradient agrees with the theoretical calculation based on the exact geometry. This scheme opens the possibility of tailoring the Casimir force using lithographically defined components of non-conventional shapes.

PACS numbers: 03.70.+k, 12.20.Fv, 12.20.Ds, 42.50.Lc

Quantum fluctuations give rise to van der Waals and Casimir forces that dominate the interaction between electrically neutral objects at nanoscale separations [1]. Under the trend of miniaturization, such quantum electrodynamical effects are expected to play an important role in nanomechanical devices. Since the first precise measurement of the Casimir force more than a decade ago [2], significant progress has been made towards the engineering and control of Casimir forces [3, 4]. For example, repulsive Casimir forces have been demonstrated in experiments involving fluids [5, 6] and predicted for vacuum gaps [7] under specific conditions. Metamaterials, with their remarkable optical properties, have also been considered as candidates for controlling the Casimir force [8, 9], but initial suggestions that the sign of the force in vacuum could be altered by metamaterials turned out to be unrealistic [10]. With regard to the non-trivial dependence of the Casimir force on the shape of the bodies [11–14], experiments involving nanostructured surfaces have demonstrated the non-pairwise additive nature of the Casimir force [15, 16]. For more complex geometries, the Casimir force has been predicted to exhibit repulsive behavior over specific distance ranges [7] or non-monotonic distance dependences [17] in multi-body geometries. Recent experiments have also measured the corrections to the Casimir force that arise from the presence of thermal fluctuations, in addition to quantum fluctuations [18].

Optical properties, geometry effects and their interplay provide powerful tools for tailoring the Casimir force. However, standard experimental schemes require an external object to be manually positioned close to either cantilevers or torsional balances [2, 6, 19–23]. Bulky micropositioners and piezoelectric actuators are used to control the separation between the two interacting bodies. Such arrangements have hindered progress in the on-chip exploitation of the Casimir force. Conventional experimental setups also face a number of other challenges. For instance, maintaining the parallelism of two flat surfaces at small distances has proven to be difficult [21]. As a result, in most experiments one of the two objects is chosen to be spherical. The alignment becomes even more challenging for nanostructured surfaces. In fact, when corrugations are present on both surfaces, it is necessary to use an in-situ imprint technique such that the patterns are automatically aligned after fabrication [16]. Another major difficulty in measuring the Casimir force at room temperature is the long-term drift in the distance between the surfaces: since the distance from the two interacting elements to their common point of support typically measures at least a few centimeters, temperature fluctuations lead to uncontrollable distance variations, limiting the duration of measurement

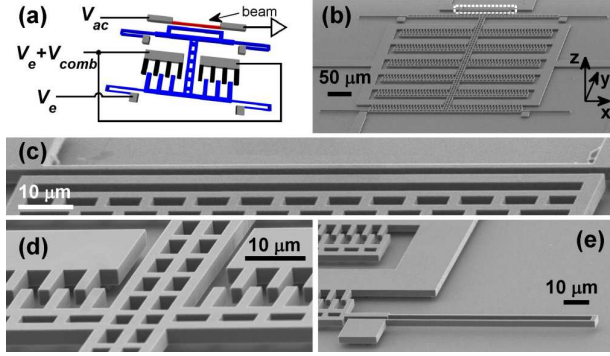


FIG. 1. (color online). The set-up of the experiment and device. (a) A simplified schematic (not to scale) of the beam, movable electrode and comb actuator supported by four springs, with electrical connections. The current amplifier provides a virtual ground to the right end of the beam. The suspended and anchored parts of the comb actuator are shown in dark and light colors respectively. The separation d between the beam and the movable electrode was controllably reduced so that the Casimir force can be detected. (b)-(e) Scanning electron micrographs of the entire micromechanical structure (b) and close-ups of: the doubly clamped beam (c), zoomed into the white dashed box in (b); the comb actuator (d) and the serpentine spring (e).

and hence the force resolution.

In this Letter, we demonstrate that the Casimir force can be the dominant interaction between single-crystalline silicon components on a semiconductor chip, in the absence of external objects. The geometry involves two microfabricated beams with near-square cross sections, the distance between which can be decreased from $1.8 \mu\text{m}$ to $\sim 260 \text{ nm}$. Both the force-sensing element and the actuator that controls the distance are integrated on the same substrate. No external alignment of the interacting bodies is necessary because they are defined in a single lithographic step. Another advantage is that the distance of the interacting elements to their common support is reduced to $\sim 70 \mu\text{m}$, about a factor of 1000 smaller than conventional experiments. The improved mechanical stability minimizes long-term drifts in the gap between the interacting objects ($< 10^{-5} \text{ nm s}^{-1}$). Furthermore, this scheme also opens opportunities for future experiments to investigate the Casimir force using lithographically defined structures of non-conventional shapes.

Figures 1(a) and (b) show a simplified schematic of the structure and a scanning electron micrograph of sample A, respectively. The element for sensing the force is a doubly-clamped

silicon beam that is $100\ \mu\text{m}$ long and $\sim 1.42\ \mu\text{m}$ wide, depicted in the top parts of Figs. 1(a) and (b). Figure 1(c) zooms in on the micro-beam. A silicon electrode of width $2.80\ \mu\text{m}$ is positioned close to the beam, as shown in the lower part of Fig. 1(c). Both the beam and the electrode are fabricated from the device layer of the same silicon-on-insulator wafer so that they have identical thickness ($2.65\ \mu\text{m}$) and distance from the substrate ($2.0\ \mu\text{m}$). Electrostatic and/or Casimir forces are exerted by the electrode on the beam depending on the voltage V_e between them. The gap between the beam and the electrode is created by deep reactive ion etching while the beam and the electrode are protected with an etch mask. With the etch mask defined by electron beam lithography, a high degree of parallelism is ensured between the beam and the electrode, without any need for manual alignment prior to force measurement.

The electrode is attached to a comb actuator so that it can be controllably moved along the y direction, reducing the separation d between the electrode and the beam from $1.92\ \mu\text{m}$ down to $\sim 260\ \mu\text{m}$ while maintaining parallelism (see Supplemental Material). Figure 1d shows a close-up of part of the comb actuator. The comb actuator consists of a set of movable comb fingers supported by four serpentine springs [Fig. 1(e)], one at each corner of the structure [Fig. 1(a)]. A second set of comb fingers [the solid structures in Fig. 1(d) with no etch holes] is fixed to the substrate on one end. When a voltage V_{comb} is applied to the fixed comb relative to the movable comb, an electrostatic force parallel to the substrate is generated. The movable combs are displaced towards the beam until the restoring force from the four springs balances the electrostatic force. As a result, the separation d is reduced as V_{comb} increases. It should be noted that the electrostatic force between the fixed and movable combs merely serves to set d . As explained below, the potential difference between the beam and the movable electrode V_e can be controlled separately, independent of V_{comb} .

The suspended beam acts as a resonant force sensor. Using the magnetomotive transduction technique (see Supplemental Material), the resonant frequency of the fundamental in-plane mode of the beam ω_R is measured to be $7.26185 \times 10^6\ \text{rad s}^{-1}$. When the movable electrode approaches the beam, ω_R shifts by an amount $\Delta\omega_R$ that is proportional to the force gradient $F'(d)$:

$$\Delta\omega_R = KF'(d), \quad (1)$$

where K is a proportionality constant. Similar to conventional experiments on Casimir forces, we also need to perform a calibration procedure by applying a voltage V_e between

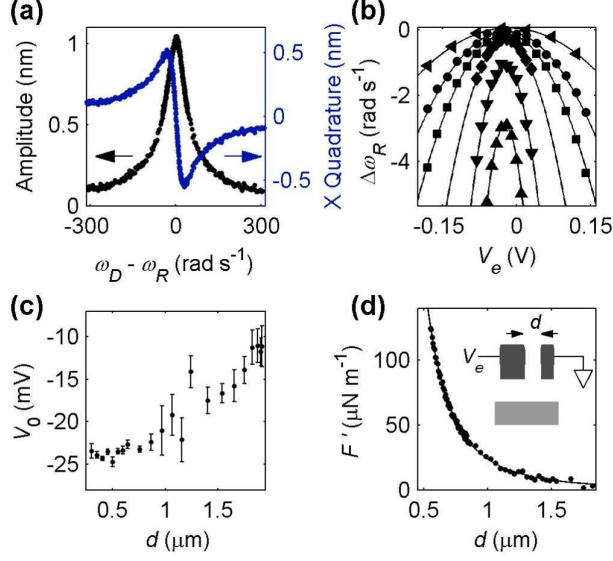


FIG. 2. (color online). Calibration of the device using electrostatic force gradient. (a) Oscillation amplitude of the beam and its X quadrature that is in phase with the periodic driving force. Shift in the resonant frequency of the beam measures the force gradient. (b) Measured frequency shift $\Delta\omega_R$ as a function of electrode voltage V_e , at $d = 1.403$ μm , 1.065 μm , 865 nm, 643 nm, 450 nm and 349 nm, from top to bottom. (c) Measured dependence of the residual voltage as a function of d . (d) Measured electrostatic force gradient on the beam (circles) at $V_e = V_0 + 100$ mV. The line represents a fit to the values calculated using finite element analysis. Inset: cross-sectional schematic of the beam, electrode and substrate with dc electrical connections.

the beam and the movable electrode to generate an electrostatic force F_e between them. F_e is proportional to $(V_e - V_0)^2$, where V_0 is the residual voltage. V_0 is measured by identifying V_e at which the maximum of the parabolic dependence of $\Delta\omega_R$ occurs. Figure 2(c) shows that V_0 is measured to be about -25 mV at small d . Over the full range of distances, V_0 changes by about 15 mV, comparable to previous experiments in the lens-plate [24] and sphere-plate [25] geometries. Even though both the beam and the electrode are made of single-crystal silicon on the same wafer, the residual voltage is non-zero. The distance dependence likely originates from adsorbed impurities and/or the etching profile (see Supplemental Material) exposing patches of different crystal orientations at the sidewalls with non-uniform potentials.

In conventional Casimir force experiments, the extension of the piezoelectric element is either pre-calibrated or directly measured. At the same time, the initial distance between the two interacting surfaces is an unknown that needs to be determined by the application

of electrostatic forces. In our experiment, distance calibration is performed using a slightly different procedure. Here, d is given by:

$$d = d_0 - \alpha V_{comb}^2, \quad (2)$$

where d_0 is the initial separation, V_{comb} is the voltage of the fixed combs relative to the movable combs and $\alpha = \frac{1}{2k_{//}} \frac{dC_{comb}}{dy}$ is a proportionality constant to be determined by fitting. $k_{//}$ is the spring constant of the serpentine springs along y . $\frac{dC_{comb}}{dy}$, the spatial derivative of the capacitance between the fixed and the movable combs, remains almost constant as the movable combs are displaced. One main difference from previous experiments is that d_0 is not a fitting parameter. Instead, d_0 is accurately measured to be $1.92 \pm 0.015 \mu\text{m}$ using a scanning electron microscope (see Supplemental Material). The dependence of F_e on the distance d is calculated using finite element analysis with our device geometry. By fitting to the calculated electrostatic force gradient $F'_e(d)$ given by Eqs. (1) and (2) for six sets of data with V_e ranging from $V_0 + 100 \text{ mV}$ to $V_0 + 150 \text{ mV}$, we obtain $\alpha = 10.55 \pm 0.04 \text{ nm V}^{-2}$ and $K = -5.38 \pm 0.10 \times 10^4 \text{ rad m s}^{-1} \text{ N}^{-1}$. In Fig. 2c, d is controlled by increasing V_{comb} from 0 to 11.375 V according to Eq. (2). Figure 2(d) plots the electrostatic force gradient on the beam as a function of d at $V_e = V_0 + 100 \text{ mV}$. The contributions of the Casimir force to the measured frequency shift ($\sim 7\%$ at $d = 0.55 \mu\text{m}$) has been subtracted. When V_e is applied, the effective distance for the electrostatic force changes because of carrier depletion. However, due to the high carrier concentration ($7 \times 10^{18} \text{ cm}^{-3}$), this change is small ($< 1 \text{ nm}$) and negligible compared to the uncertainty in d .

Next, we set $V_e = V_0$ and measure the force gradient F'_c between the beam and the electrode as a function of d [Fig. 3(a)]. The thick solid line represents the theoretical values of the Casimir force calculated for silicon structures of such geometry with no fitting parameters. It includes the contributions of the finite conductivity of silicon and the imperfect etching profiles on the sidewalls ($\sim 88^\circ$ from the substrate surface, see Supplemental Material). This calculation involves a boundary-element method (BEM) discretization of the beam and substrate surfaces, combined with a recent fluctuating-surface-current formulation of the Casimir force between dielectric bodies that writes the full Casimir-energy path integral as a simple expression in the classical BEM interaction matrix [13]. Neglecting the finite length of the beams, the geometry here reduces to a 2D problem in the cross sections (integrated over the longitudinal wavevector), and each object's surface is discretized into set

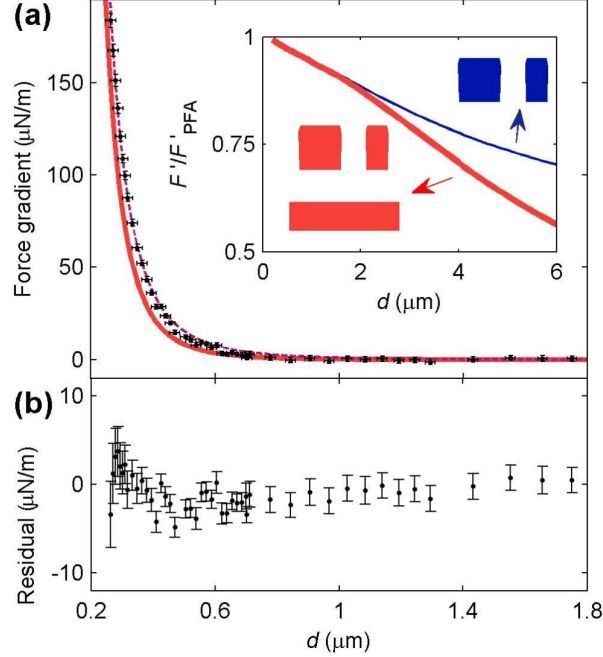


FIG. 3. (color online) Measured Casimir force gradient F'_c between the beam and the movable electrode as a function of separation d . (a) The thick solid line represents the calculated Casimir force gradients between an electrode and a beam made of silicon. The thin dashed line includes possible contributions from patch potentials. Inset: The ratios of the calculated Casimir force between the beam and the electrode to the forces given by the PFA are plotted as the thick (with substrate) and thin lines (without substrate). (b) Deviations of the measured force gradient from the dash line in (a).

of line segments described by "rooftop" basis functions [26]. We found that a discretization of approximately 3200 total points for all surfaces and a substrate truncated to 1 μm was sufficient to obtain convergence to 1% accuracy. In the calculations, the dielectric function of silicon $\epsilon(i\xi)$ is obtained using the Kramers-Kronig relations with the tabulated optical constants for frequency > 5000 rad s^{-1} . For $\xi < 5000$ rad s^{-1} , $\epsilon(i\xi)$ is given by:

$$\epsilon(i\xi) = 1.0035 + (11.87 - 1.0035)/(1 + \xi^2/\omega_0^2) + \omega_p^2/[\xi(\xi + \Gamma)], \quad (3)$$

where $\omega_0 = 6.6 \times 10^{15}$ rad s^{-1} , $\omega_p = 2.5562 \times 10^{14}$ rad s^{-1} and $\Gamma = 6.364 \times 10^{13}$ rad s^{-1} .

Unlike the sphere-plate configuration, the roughness on the sidewalls cannot be directly measured and is not included for the solid line in Fig. 3(a). From the top view micrograph of the beam and electrode, we determine the rms roughness of the edges to be 12 nm, mainly

due to non-uniformity of the electron beam lithography. Using Eq. 16 in Ref. [27] and the proximity force approximation (PFA), the roughness correction is estimated to be about 3% of the Casimir force at the closest distance [27]. Despite the imperfect agreement between measurement and theory, it is clear that the Casimir force becomes the dominant interaction between the beam and the movable electrode at small d .

One plausible explanation for the deviations between measurement and theory involves residual electrostatic forces that are associated with patch potentials. Following the analysis of Ref. [28], such residual forces display similar distance dependence as the applied electrostatic force, but varies as $[V_0(d) + V_1]^2 + V_{rms}^2$. The first term originates from the spatial variations in the contact potential that give rise to a distance dependent V_0 while the second term accounts for patches smaller than the effective interaction area. Currently, our experiment lacks the sensitivity to resolve the force gradients at $d > 0.8 \mu\text{m}$. Therefore, unlike Ref. [28], we cannot measure long range residual electrostatic forces and fit at distances where the Casimir force is negligible. Instead, we fit the measured force gradients to the calculated Casimir force gradient modified by residual electrostatic forces due to patch potentials [thin dashed line in Fig. 3(a)]. By setting $V_1 = -V_0 = 11.3 \text{ mV}$ at the largest d , we obtain a fitted value of $V_{rms} = 16.8 \text{ mV}$.

The Casimir force gradient between a beam and an electrode with near-square cross sections has not been measured experimentally before. This configuration opens the possibility of testing a number of fundamental concepts. One important question is the validity of the PFA. The inset of Fig. 3(a) compares the Casimir force gradient generated by the PFA to calculations of the exact geometry of the silicon structures. The ratio decreases with distance, reaching 56% at $6 \mu\text{m}$. Secondly, this geometry could offer a direct demonstration of the non-pairwise nature of the Casimir force. The inset of Fig. 3(a) shows that the calculated Casimir force between the beam and the electrode depends on the presence of a third body, the substrate. When the substrate is removed, the Casimir force increases by 14% at $6 \mu\text{m}$. Recent theoretical analysis also predicted that the Casimir force between the beams exhibits a non-monotonic dependence on the distance to the substrate that cannot be explained by pairwise additive models of the force [17]. Since the Casimir force gradient at these distances is beyond the reach of the current setup, future experiments to reveal the aforementioned effects would require more sophisticated measurement circuitry or other detection schemes [29] to improve the sensitivity at large ($> 2 \mu\text{m}$) separations.

We have shown that the Casimir force can be the dominant interaction between silicon micromechanical components on a semiconductor chip, in the absence of external objects. Our results represent the first step towards on-chip exploitation of the Casimir force. The compact and integrated actuation and detection platform also provides new opportunities of tailoring the Casimir force using geometry effects. Structures are defined by electron beam lithography, making it possible to create surfaces with complex shapes [30] that are automatically aligned after fabrication. Nevertheless, much progress will be necessary, particularly in sample fabrication and characterization, to achieve the $< 5\%$ agreement between theory and measurement [18, 19, 22] that has been claimed in conventional Casimir force experiments between spheres and plates.

H.B.C., J.Z., Z.M. and Y.B. were supported by DOE No. DE-FG02-05ER46247 and NSF No. DMR-0645448. H.B.C. is supported by Shun Hing Solid State Clusters Lab and HKUST 600511 from the Research Grants Council of Hong Kong SAR. S.G.J., A.W.R., and A.P.M are supported in part by DARPA under contract N66001-09-1-2070-DOD. M.T.H.R. was supported by the Singapore-MIT Alliance's Program in Computational Engineering. A portion of this research was conducted at the Center for Nanophase Materials Sciences, which is sponsored at Oak Ridge National Laboratory by the Office of Basic Energy Sciences, U.S. Department of Energy.

* hochan@ust.hk

- [1] H. B. G. Casimir, Proc. Kon. Ned. Akad. Wet. **51**, 793 (1948).
- [2] S. K. Lamoreaux, Phys. Rev. Lett. **78**, 5 (1997).
- [3] G. L. Klimchitskaya, U. Mohideen, and V. M. Mostepanenko, Rev. Mod. Phys. **81**, 1827 (2009).
- [4] A. W. Rodriguez, F. Capasso, and S. G. Johnson, Nat. Photonics **5**, 211 (2011).
- [5] I. E. Dzyaloshinskii, E. M. Lifshitz, and L. P. Pitaevskii, Adv. Phys. **10**, 165 (1961).
- [6] J. N. Munday, F. Capasso, and V. A. Parsegian, Nature **457**, 170 (2009).
- [7] M. Levin, A. P. McCauley, A. W. Rodriguez, M. T. H. Reid, and S. G. Johnson, Phys. Rev. Lett. **105**, 090403 (2010).
- [8] U. Leonhardt and T. G. Philbin, New J. Phys. **9**, 254 (2007).

- [9] R. Zhao, J. Zhou, T. Koschny, E. N. Economou, and C. M. Soukoulis, *Phys. Rev. Lett.* **103**, 103602 (2009).
- [10] A. P. McCauley, R. K. Zhao, M. T. H. Reid, A. W. Rodriguez, J. F. Zhou, F. S. S. Rosa, J. D. Joannopoulos, D. A. R. Dalvit, C. M. Soukoulis, and S. G. Johnson, *Phys. Rev. B* **82**, 165108 (2010).
- [11] A. Lambrecht, P. A. M. Neto, and S. Reynaud, *New J. Phys.* **8**, 243 (2006).
- [12] S. J. Rahi, T. Emig, N. Graham, R. L. Jaffe, and M. Kardar, *Phys. Rev. D* **80**, 085021 (2009).
- [13] M. T. H. Reid, A. W. Rodriguez, J. White, and S. G. Johnson, *Phys. Rev. Lett.* **103**, 040401 (2009).
- [14] P. S. Davids, F. Intravaia, F. S. S. Rosa, and D. A. R. Dalvit, *Phys. Rev. A* **82**, 062111 (2010).
- [15] H. B. Chan, Y. Bao, J. Zou, R. A. Cirelli, F. Klemens, W. M. Mansfield, and C. S. Pai, *Phys. Rev. Lett.* **101**, 030401 (2008).
- [16] H. C. Chiu, G. L. Klimchitskaya, V. N. Marachevsky, V. M. Mostepanenko, and U. Mohideen, *Phys. Rev. B* **81**, 115417 (2010).
- [17] A. Rodriguez, M. Ibanescu, D. Iannuzzi, F. Capasso, J. D. Joannopoulos, and S. G. Johnson, *Phys. Rev. Lett.* **99**, 080401 (2007).
- [18] A. O. Sushkov, W. J. Kim, D. A. R. Dalvit, and S. K. Lamoreaux, *Nat. Phys.* **7**, 230 (2011).
- [19] U. Mohideen and A. Roy, *Phys. Rev. Lett.* **81**, 4549 (1998).
- [20] H. B. Chan, V. A. Aksyuk, R. N. Kleiman, D. J. Bishop, and F. Capasso, *Science* **291**, 1941 (2001).
- [21] G. Bressi, G. Carugno, R. Onofrio, and G. Ruoso, *Phys. Rev. Lett.* **88**, 041804 (2002).
- [22] R. S. Decca, D. Lopez, H. B. Chan, E. Fischbach, D. E. Krause, and C. R. Jamell, *Phys. Rev. Lett.* **94**, 240401 (2005).
- [23] J. Laurent, H. Sellier, A. Mosset, S. Huant, and J. Chevrier, *Phys. Rev. B* **85**, 035426 (2012).
- [24] W. J. Kim, M. Brown-Hayes, D. A. R. Dalvit, J. H. Brownell, and R. Onofrio, *Phys. Rev. A* **78**, 020101 (2008).
- [25] G. Torricelli, P. J. van Zwol, O. Shpak, C. Binns, G. Palasantzas, B. J. Kooi, V. B. Svetovoy, and M. Wuttig, *Phys. Rev. A* **82**, 010101 (2010).
- [26] M. T. H. Reid, Phd thesis, Massachusetts Institute of Technology (2010).
- [27] M. Bordag, G. L. Klimchitskaya, and V. M. Mostepanenko, *Phys. Lett. A* **200**, 95 (1995).
- [28] W. J. Kim, A. O. Sushkov, D. A. R. Dalvit, and S. K. Lamoreaux, *Phys. Rev. Lett.* **103**,

060401 (2009).

[29] D. Van Thourhout and J. Roels, *Nat. Photonics* **4**, 211 (2010).

[30] A. W. Rodriguez, J. D. Joannopoulos, and S. G. Johnson, *Phys. Rev. A* **77**, 062107 (2008).